Seismic Wave Propagation in and Around Boreholes

by

Tiepeng Zhou

B.S., Huazhong University of Science and Technology, China (1985)

Submitted to the Department of Earth, Atmospheric, and Planetary Sciences
in partial fulfillment of the requirements for the degree of

Master of Science

at the

MASSACHUSETTS INSTITUTE OF TECHNOLOGY

September 1995

Signature of Author .....
Department of Earth, Atmospheric, and Planetary Sciences
1995

Certified by .....
M. Nafi Toksöz
Professor of Geophysics
Thesis Advisor

Certified by .....
Richard L. Gibson, Jr.
Research Scientist
Co-Thesis Advisor

Accepted by .....
Thomas H. Jordan
Department Head
Department of Earth, Atmospheric, and Planetary Sciences

Seismic Wave Propagation in and Around Boreholes

by

Tiepeng Zhou

Submitted to the Department of Earth, Atmospheric, and Planetary Sciences
on 1995, in partial fulfillment of the
requirements for the degree of
Master of Science

Abstract

Seismic imaging applications using a source or receiver in a borehole are significantly complicated by the coupling of the wavefields propagating in the formation with those in the borehole. In particular, a borehole source can generate a very large amplitude Stoneley wave, and a borehole receiver will record both incoming body waves and tube waves generated by the interaction of these waves with the receiver borehole. These problems are particularly severe when the source and receiver are in the same borehole, the single-well imaging configuration. In this thesis we have explored ways of using conventional, staggered-grid finite difference codes to model these wave propagation effects to help understand data that may be collected in such experiments.

The most fundamental problem in simulating these effects with finite difference algorithms is that both the borehole and the surrounding medium must be discretized, and a modeling scheme that must finely discretize the small borehole (diameter about 0.20 m) will not be able to incorporate large models (on the order of 100 m) around the borehole because of the sheer size of the resulting discretized model. We therefore show results of tests demonstrating that it is possible to relax these constraints somewhat in two ways: (1) at lower frequencies (i.e., wavelength in the formation is relatively large compared to the borehole), the borehole need not be discretized as finely to accurately reproduce the same effects on source wavefields as a fine discretization, and (2) as long as the wavelength remains fairly large compared to the borehole, the size of the borehole can be increased without significantly altering the radiation pattern. Both finite difference and stationary phase radiation pattern results confirm the second point.

The second issue we address is the problem of tube waves recorded in single-well imaging experiments. One way of helping to suppress the effects of these waves on receivers, especially hydrophones, is to place damping devices within the borehole between source and receivers. We use the finite difference method to simulate the effects of dampers of various velocities and lengths. In general, the larger the velocity

contrast between the damper and the fluid, the more the tube wave is suppressed. Likewise, a longer damper will also better suppress the tube wave. In contrast, at least for realistic values, the center frequency of the source does not influence the effectiveness of the damper very much. One very important consideration we prove with the calculations is that the use of multiple dampers is very effective, suggesting that an effective procedure in the field may involve placing two or more dampers between source and receiver.

Thesis Advisor: M. Nafi Toksöz
Title: Professor of Geophysics

Co-Thesis Advisor: Richard L. Gibson, Jr.
Title: Research Scientist

Acknowledgments

Life is good, especially when the thesis is finished!

I would like to thank my wife, Mandi Wang. Without her love, constant encouragement, patience and support, I could not have survived the most stressful time of my life.

I would also like to thank my advisor, Prof. Nafi Toksöz, for guidance and patience which enabled me to finish this thesis. I greatly benefited from his thoughts and insights on borehole geophysics and seismic wave propagation.

I am grateful to Rick Gibson. Though I can't remember how many questions I asked him and how long he spent teaching me the essentials of geophysics, I do remember that he was always enthusiastic and was my constant source of consulting. His help extended far beyond seismology and borehole geophysics.

My former office mate and best friend, Wenjie Dong, introduced me to the field of borehole geophysics and continues to be a stimulus for me to work hard. I appreciate and am thankful for his friendship and understanding.

Additional appreciation is given to my mentor, Dr. Zhenya Zhu, who discussed everything with me; Ningya Cheng, who taught me the beauty of the finite difference method; and Jie Zhang, Xiaomin Zhao, Guo Tao, and Weiqun Shi, who were always there when I needed help.

Special thanks to Prof. Dale Morgan and Dr. David Lesmes, who taught me rock physics and the importance of cooperation and communication in scientific research; Arthur Cheng, who presented me with a best life motto; Joe Matarese, Chuck Doll, and Jane Maloof for their help in network problems and software; Roger Turpening for all the books and journals he put in the Lab's library (in fact, I use them very frequently); Liz Henderson, Sue Turbak, and Naida Buckingham. Naida helped edit my paper and Liz did the painstaking formatting of this thesis.

Thanks to all my friends and colleagues in the laboratory: Bill Rodi, Yingping Li, Bob Greaves, Antonio De Lilla, Cheo Lee, Laurence Jouniaux, Francesca Scire-

Scappuzzo, and Matthijs Haartsen.

Personally, I am indebted to my cousins, An Yang and Jing Wang, whose friendship made my life at MIT much easier, and to my parents, my brothers and sister, who have always given me the mental and emotional support to seek my dreams!

Contents

Chapter 1

Introduction

1.1 Objective

An important task of borehole geophysics is the use of full-waveform seismic data to infer subsurface structures. Conventional sonic borehole measurements focus mainly on primary sonic arrivals such as refractional compressional P-waves, refractional shear S-waves and borehole Stoneley mode arrivals. These methods are only effective in the assessment of near borehole formation properties.

In this thesis, we propose methods to effectively utilize three-dimensional finite difference method to simulate seismic wave propagation in and around a borehole. Also we propose methods for modelling the effects of tube wave dampers on artificial attenuation of the dominant borehole tube waves. The goal of this work is to develop methods that can eventually be applied to the task of simulating single-well imaging experiments.

1.2 Background

Crosshole tomography can provide finer substructure details and utilize reflection information from boundaries outside the borehole. A variety of full-waveform crosshole

imaging approaches have been proposed, ranging from VSP-CDP mapping (Baker and Harris, 1984; Iverson, 1988; Abdalla *et al.*, 1990), to migration (Hu *et al.*, 1988), to acoustic diffraction tomography (Devaney, 1984; Wu and Toksöz, 1987, Lo *et al.*, 1988; Pratt and Worthington, 1990a) or elastic diffraction tomography (Beydoun *et al.*, 1989; Pratt and Worthington, 1990b; Dickens, 1994). One of the major difficulties concerning these techniques is the lack of understanding of the seismic signatures radiated from various seismic sources placed downhole. Another problem is the accurate time-picking of arrivals. Many of these methods don't consider the influence of receiver boreholes and assume a constant velocity background with weak scatters. Additionally, crosshole tomography is much more expensive than single-well tomography.

There is also some increasing interest in single-well imaging. Hornby (1989) observed reflected P- and S-wave signals originating from dipping boundaries away from the borehole and, using an algorithm based on a depth migration before stack, formed a high resolution image of the near-borehole bedding features. He also applied his method to more complex geologic settings (Hornby, 1993). The method used the 2-D finite difference method to simulate borehole refracted arrivals and to detect velocity vertical variations. Although it can be applied to detect lateral velocity variations in the horizontal well case, it is limited to very near borehole surroundings and a high frequency assumption. Thus the waves in the borehole behave like classic rays and Stoneley waves are relatively weak and, consequently, the refracted wave is highlighted.

Exxon (Chen *et al.*, 1994) recently designed a single-well profiling tool suitable for imaging steeply dipping geologic structures, horizontal well imaging, and low-frequency logging. In their illustrations of these tools, the designers suggested that by varying the spacing between the source and the receivers, one can record the reflection signals within data windows where the tube wave is either absent or minimal. The primary P wave propagates parallel to the vertical borehole axis, while the reflected P

wave has both horizontal and vertical components. Data recorded on the horizontal components can be used to more easily differentiate a reflected arrival from a direct P wave arrival. By using an array of three-component geophones, reflected arrivals can thus be detected, especially when they arrive before tube waves. However, if the formation is a slow formation, and the source-receiver spacer is not long, the Stoneley wave will come before the reflected arrivals. Because the reflected arrivals are much weaker than the tube waves, one will not be able to detect the reflections.

A complete analysis of single-well imaging is, however, not possible without understanding the borehole radiation and reception patterns and the interaction of seismic waves with boreholes. The single-well imaging problem is more complicated than cross well imaging, because the source and receivers are in the same borehole. In this case, tube waves and primary refracted arrivals are the two dominant waves and separation of the reflections from them in seismic data processing is thus difficult.

The first study of the effect of a borehole on an explosive source was done by Heelan (1953). He studied the P and S-wave radiation from an explosive source in an empty borehole of finite length embedded in a homogeneous elastic medium. Lee and Balch (1982) extended Heelan's work by considering a fluid in the borehole and used the stationary phase method in deriving a low frequency approximation. Meredith *et al.* (1990) developed both numerical and analytical solutions to describe radiation from a downhole source in the near and far field for a variety of downhole and sources, and identified the Mach wave radiation in a slow formation. The stationary phase formulation is also employed by Gibson (1994) in studying radiation from a source in a cased borehole, where the stationary phase wavenumber is determined analytically and the boundary condition equations are solved numerically. Dong *et al.* (1992) investigated the source borehole effect on downhole source radiation in homogeneous and heterogeneous anisotropic layered media. He gave analytical approximations and numerical modeling using the boundary element method from various downhole sources in different boreholes. Peng (1993) made a complete and

systematic investigation of the borehole receiver coupling theory. He studied the borehole effects on downhole seismic measurements. He also developed numerical solutions to take them into account and processing techniques to remove them from field data.

Considering the various algorithms for full waveform numerical simulation, the finite difference method is one that can't be ignored. The finite difference method (FDM) has been widely used since digital computers became available. High-speed and massively parallel computer machines now make it possible to use FDM to simulate very complex geologic structures. However, because the finite difference method requires that the entire physical space of the earth model be discretized, the most limiting factor is the size of the model which can be considered relative to the shortest seismic wavelengths that are present. This limitation makes it difficult to study the propagation of high frequency seismic energy at great distances from the source, especially in 3-D situations. Both the computation time and the computer memory requirements become important in the computation of synthetic seismograms for 3-D earth models. There exists a large scale difference between the borehole geometry and the surrounding formations so that the finite difference method is numerically very expensive. In this case, saving memory and enhancing grid step sizes becomes significant.

1.3 Outline

Chapter 2 gives first a summary description of the implementation of the three-dimensional finite difference method (FDM). Then we discuss two methods to more effectively utilize the finite difference method. The basic goal of these methods is to use fewer grid points to model a larger model. The first method is to coarsely discretize the borehole to enhance grid step size; the second is to use a larger borehole and higher frequency. We find that in the low source frequency range, both in a

hard formation and a soft formation, a coarse borehole discretization will not affect the computed borehole radiation pattern. If we use four points for the borehole discretization instead of fifteen points discretization (Cheng, 1994), a tremendous amount of computing time will be saved. In addition, if the borehole radius is much less than the borehole fluid wavelength, the radiation patterns of two different size of boreholes are very similar to each other. Hence, a larger borehole can be used in the modeling, further increasing the discretization spacing.

Chapter 3 then discusses the use of dampers to simulate the attenuating of the Stoneley wave. The goal is to explore ways to highlight the reflected arrivals in single-well applications. The dampers are modeled as simple, solid material hollow cylinders in the borehole. We investigate the effects of block length, width and block material property on attenuating Stoneley waves, at both low and high frequency and in soft and hard formation cases. We find that a hard rigidity formation has a strong effect on attenuating tube waves. The reflected energy of the Stoneley wave is proportional to the block top area. The longer a block, the stronger an effect it has on the attenuating of Stoneley waves. But when the length reaches a specific value (about 1/4 Stoneley wavelength), the effect will not increase. The same applies to the block material and the block width.

Conclusions are provided in Chapter 4 along with an outline of the future direction of our research.

Chapter 2

Effective Finite Difference Method

2.1 Introduction

The limiting factor of the use of the finite difference method to simulate borehole acoustic wave propagation is the large scale difference between the borehole size and the surrounding formation. The borehole radius is usually about 20 cm and the seismic wavelength on the order of meters. A fine discretization of borehole requires that the grid size be less than a tenth of the borehole radius, or namely in order of centimeters. It is impossible to use a grid size of the order of centimeters to simulate a model of tens of meters.

A number of finite difference methods have been proposed to circumvent this difficulty. However, most of them do not directly treat boreholes. The stress around the borehole is calculated separately or other methods are used. Two representative ones are the receiver borehole coupling method (Peng, 1993) and the equivalent source/receiver array method (Kurkjian *et al.*, 1994).

Peng developed his borehole coupling method for cross well tomography. His method decomposes the finite difference simulation into two parts: compute the stress fields in the vicinity of the presumed borehole locations, and apply the borehole coupling theory thereafter to obtain the pressure in the borehole fluid. Peng's method

reasonably ignored the effects of the source borehole, because his applications were to VSP experiments. However, this is not true for the single-well imaging, in which the source borehole and receiver borehole are identical. The dominant waves in the borehole are the primary arrivals (Stoneley wave and the refracted waves) excited directly by the source. The waves generated by the incident reflections are very weak compared to the primary arrivals, and are hard to identify and separate from the dominant borehole waves.

Again, the equivalent source/receiver array method (Kurkjian *et al.*, 1994) is suitable for cross hole tomography. The source borehole and the receiver borehole are represented by a distributed seismic source/receiver. Finite difference method is used to compute the body wavefield between the source and receiver borehole. The waves that reach the receiver borehole are the body waves excited by the source borehole. And the effect of the source borehole waves is negligible at receivers in most cases. However, their method must be altered for single-well applications so that it is a bit complicated to utilize their method. it difficult for accurate simulation of borehole primary arrivals.

The work in this thesis is motivated by the characteristics of the single-well imaging. A single-well imaging problem can be divided into four parts: (1) the radiation pattern of the source that determine the waves that escape the source borehole and propagate to the far-field formation; (2) the propagation of the waves in 3-D medium that encounter the dipping formation subsurfaces and reflect back to the borehole; (3) the reception pattern that determines the interaction of borehole, the reflected waves with the borehole; and (4) the interaction of the primary borehole waves and the reflected waves. To simulate these effects, we develop a finite difference method that, unlike the above mentioned methods, directly treats the boreholes. In particular, we circumvent the limiting factor of the scale difference between borehole and formation by using a coarser borehole discretization and a larger borehole.

The finite difference method requires that the entire space be discretized, and the

fluid borehole-solid formation is approximated by a polygon. To avoid the boundary scattering due to the inaccurate geometrical approximation, a fine discretization is usually required (Cheng, 1994). However, if the borehole radius is much smaller than the minimum seismic wavelength that is present, we show below that a much coarser discretization will not influence the seismic wavefield either in the borehole or in the formation. This is true for both the fast formation and slow formation. We also show that further increase in efficiency can be obtained by replacing a smaller borehole with a larger borehole yielding the same radiation pattern.

Below we first provide a brief description of the staggered-grid finite difference algorithm. After this overview, we address the efficient simulation of single-well synthetic seismograms by using the coarse discretization of the borehole. A direct comparison of different borehole discretizations proves that a coarse model is accurate. Secondly, we show that a larger borehole can also be used in the modeling as long as the ratio of wavelength to borehole radius remains fairly large.

2.2 Finite Difference Implementation

The finite difference method is based on a three-dimensional staggered grid (Virieux 1984, 1986; Cheng, 1994), using the stress-velocity first-order hyperbolic differential equations. The time domain finite difference are adopted in fourth-order accuracy in space and second-order accuracy in time. The grid dispersion and anisotropy are negligible when using a grid spacing of 10 points per wavelength (Kelly *et al.*, 1976). The stability condition is obtained by choosing the numerical velocity much larger than the maximum media physical velocity (Kelly *et al.*, 1976). A damping layer at the outside boundary is used to absorb the artificial boundary reflections. Analysis of grid dispersion and stability can be found in a number of references (Kelly *et al.*, 1976; Virieux, 1986; Levander, 1988); Analysis of the absorbing of artificial boundary reflections is discussed by Lindman (1975), Clayton and Enquist

(1977), Virieux (1986), and Higdon (1986, 1987, 1990).

Our finite difference scheme is implemented on an nCUBE-2 parallel computer in the Earth Resources Laboratory, Massachusetts Institute of Technology (Cheng, 1994). A grid decomposition algorithm is applied to minimize the internode data communications. This algorithm decomposes the whole grid into small subgrids and then maps these subgrids into nCUBE nodes. The finite difference algorithm is calculated on each subgrid. In message passing, only wave fields that are specifically used in the neighboring nodes take part in the communication.

2.3 Formation Properties

Formation properties we use in this thesis are shown in Table 2.1.

Lithology	V_p m/s	V_t m/s	ρ kg/m^3
Solenhofen Limestone	5980	3300	3300
Berea Sandstone	4000	2300	2656
Shale	2770	1230	2250
Water	1500		1000

Table 2.1: Physical properties of lithologies and materials used in this thesis. Physical properties include P-wave (V_p) and S-wave (V_s) velocities, densities (ρ). The Velocities are in meters per second, densities in kilograms per cubic meters. References are Thomsen(1986) and Peng (1993).

2.4 Borehole Discretization Effects

Our first approach to utilize the finite difference method effectively is to discretize the borehole coarsely. In low frequency range, the coarser discretization of the borehole will not influence the borehole radiation pattern and reception pattern. This is easy to explain. Intuitively, if the borehole radius is much smaller than the minimum seismic wavelength present, the roughness of the borehole boundaries will not be

"recognized" by the waves. Yet the result is numerically significant. For example, if the borehole is discretized using 3 points per radius instead of 15 points per radius (Cheng, 1994), it can handle three-dimensional model a 125 times larger, using the same CPU computing time and memory.

Figure 2.1 shows the borehole geometry we use. A source is located in the center of a fluid-filled borehole, surrounded by a homogeneous formation (shale in Table 2.1). An array of hydrophones are located along the borehole axis in the fluid and an array of geophones outside of the borehole in an array direction parallel to the borehole axis. The source is monopole, with frequency 2.0 kHz. The borehole radius is 0.15 m. The frequency and the borehole radius are so chosen that the borehole radius is much less than the minimum seismic wavelength present. We then discretize the borehole with 2, 4, 8, 12 grid points. We want to see the effects of the discretization on the radiation pattern.

Figure 2.2a is the seismogram of pressure for soft formation (shale in Table 2.1). The difference is small if we discretize the borehole with 4, 8, or 12 points. There is less than 5% difference between the results of using 2 points and using 4 points. We find that the errors in the refracted P-waves are much less than the error of the Stoneley waves. This is likely due to the difference in wavelengths of these two waves. The Stoneley wave has a smaller wavelength and will therefore be more sensitive to details of the borehole model.

Figures 2.2b and 2.2c are the particle displacement velocities along the x-direction (radial) and z-directions (vertical), which are perpendicular to and parallel to the borehole axis, respectively. The distance between the borehole axis and the receiver array is 0.3 m where the Stoneley wave still exists but has decayed. As we can see in Figure 2.2, the P-wave's amplitude decreases, the S-wave's amplitude increases and the Stoneley waves remain constant. This is expected from the radiation patterns of P and S waves from the source in the borehole. Still there is no substantial difference when the grid points per radius is 4 or larger. This means that 4 points per borehole

radius discretization is enough in general.

2.5 Effective Borehole

Figures 2.3a and 2.3b are the radiation patterns computed using the stationary phase method. The formation is fast formation (Berea Sandstone, Table 2.1). A volume injection source is used, with center frequency 600 Hz. The boreholes used have radius values 0.15 m and 0.60 m. The ratios of the borehole radius to the compressional wavelength are separately 0.0225 and 0.09. This means the borehole radius are much smaller than the formation compressional wavelength.

On the whole, if the borehole radius is much less than the minimum seismic wavelength present, the radiation patterns of boreholes of different sizes are very similar. This means that the numerical results for larger boreholes can be thus applied to numerical simulation associated with a smaller borehole if the ratio of wavelength to borehole radius is similar. This circumvents the difficulty coming from the in by large-scale difference between the borehole and its surrounding formation using FDM. It could save tremendous computing time and can handle much larger numerical models.

The radiation pattern results depend on the wavelength size relative to the borehole. The dependence of borehole wave propagation on the wavelength can be further demonstrated with an example calculation. Figures 2.4a and 2.4b show two boreholes. The first borehole has radius 0.6m and source center frequency 0.75 kHz, while the second one has borehole radius 0.15 m and source center frequency 3.0 kHz. Therefore, the ratios of the borehole radius to the wavelength in the formation are the same in these two models. The array of the receivers is defined to be a constant distance of the same number of wavelengths.

Figures 2.5a–d are the particle displacement velocities of these two source boreholes. The seismograms are identical when the distances are compared in terms of wavelengths and the time axis are scaled to take into account the change in fre-

quency. Hence, this shows that the wavelength is the physical parameter governing wave propagation in the borehole system.

2.6 Summary

We adopt two approaches to effectively utilize the finite difference method for the purpose of single-well imaging. The first one is to coarsely discretize the borehole. If the borehole radius is much less than the minimum seismic wavelength present, this method works very well for both soft formation and hard formation. The second one is to replace a smaller borehole with an effective larger borehole. Two source boreholes are called effective boreholes to each other if their radiation patterns are very similar. The radiation pattern and the borehole primary arrival modes of two effective boreholes are very similar. Both of these two approachs allow us to keep the advantages of the simplicity and explicitness of the finite difference method.

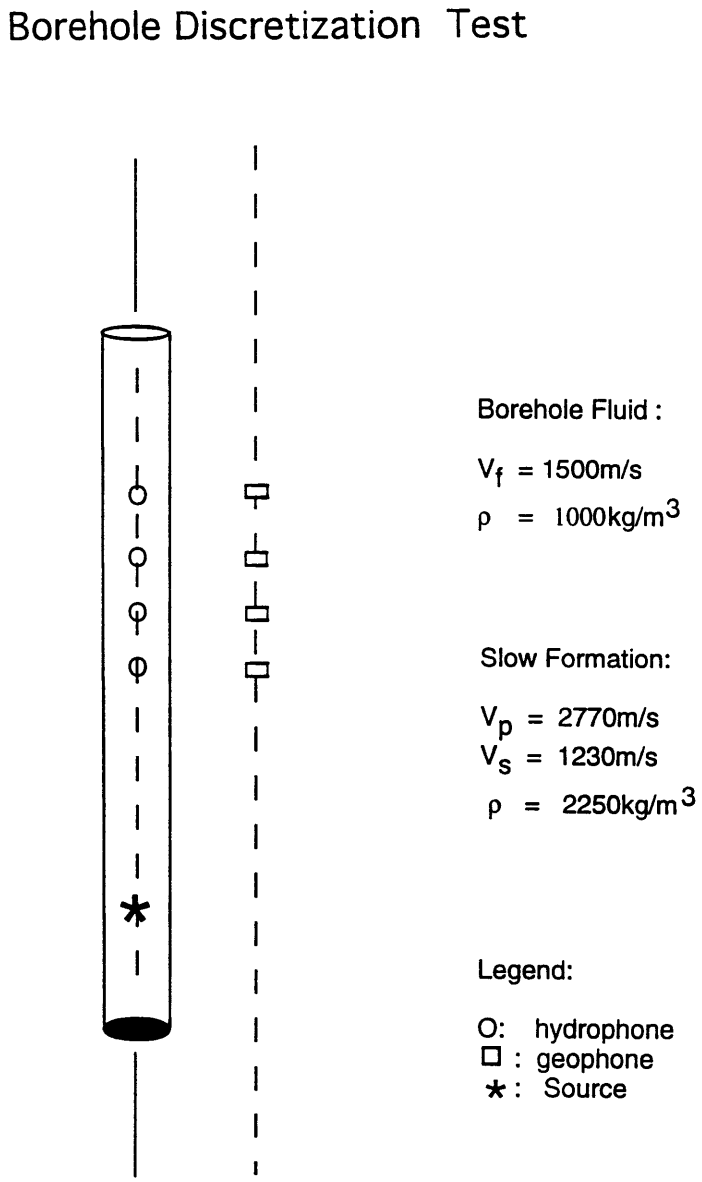

Figure 2.1: The bore discretization test. The monopole source has center frequency 2.0 kHz. The borehole radius is 0.15 m. 4 hydrophones are set in the borehole center with source-receiver-distance from 1.5 m to 1.95 m, and 4 geophones are in the solid formation. The receivers are evenly distributed with spacing 0.15 m. The distance between the two receiver arrays is 0.40 m.

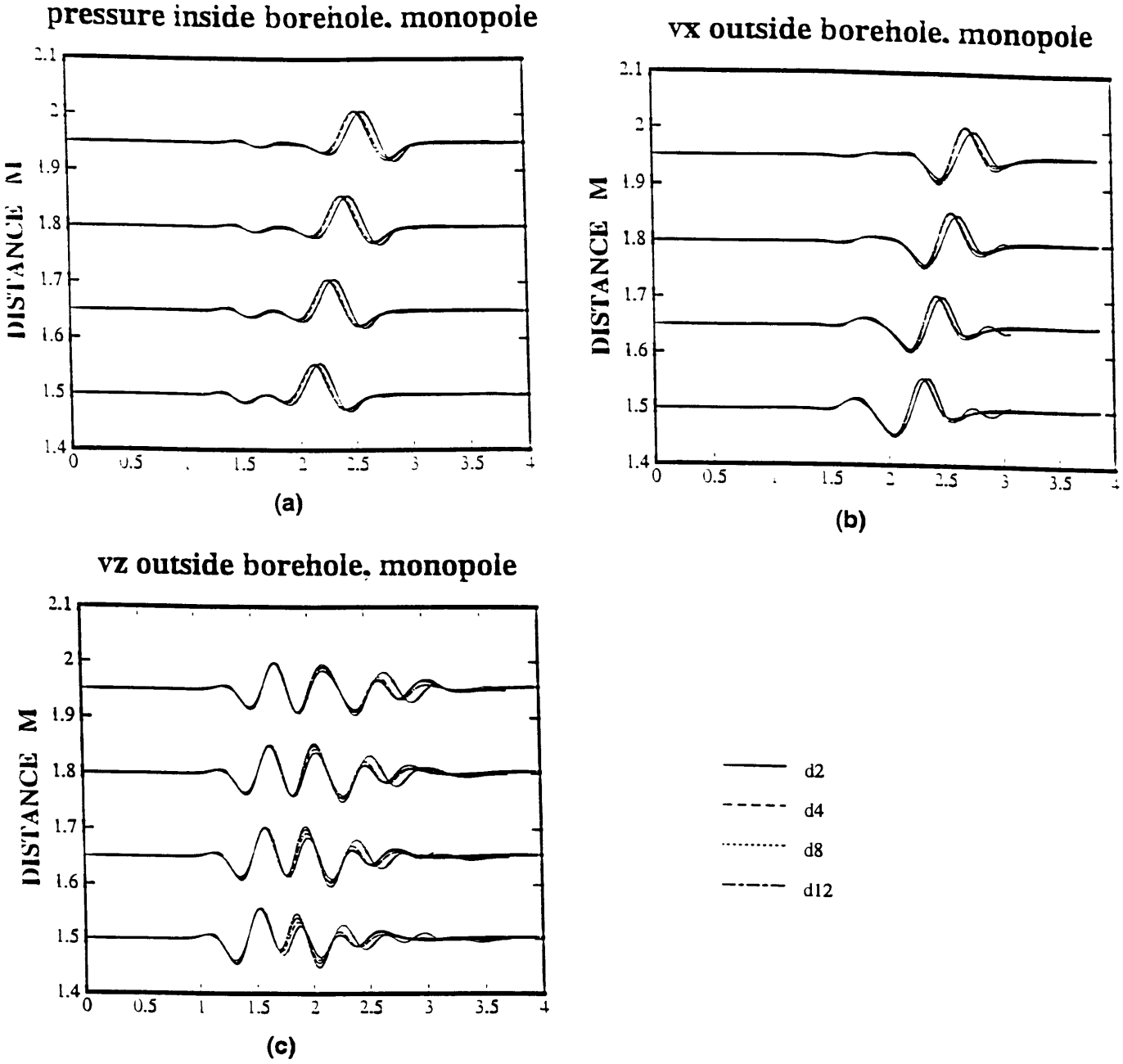

Figure 2.2: Tests of borehole discretization effects. The borehole environment is shown in Figure 2.1. Figure 2.2a is the pressure detected by the hydrophones; b,c are the radial and vertical components of particle displacement velocities detected by the geophones in solid formation.

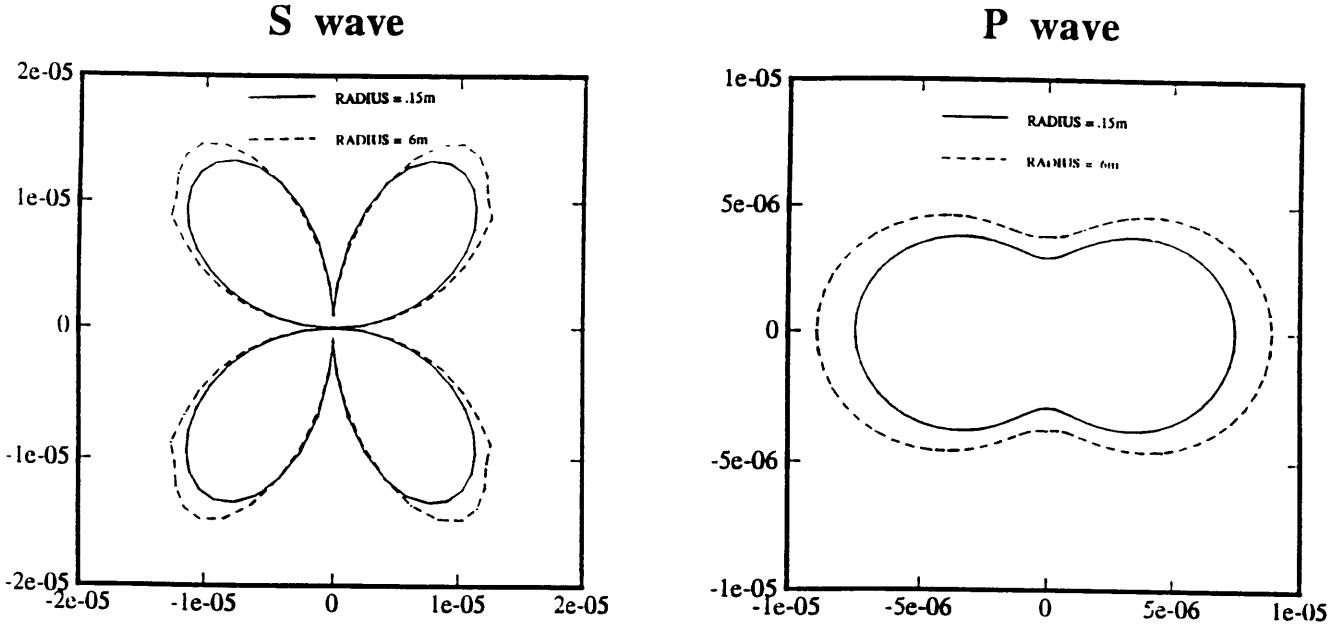

Figure 2.3: Radiation patterns computed by the stationary phase method (Gibson, 1994). The monopole source, with center frequency 600 Hz, is located in the center of fluid-filled borehole of radius 15 cm and 60 cm. a and b are the shear and compressional wave radiation pattern. The fast formation is the Berea Sandstone (Table 2.1).

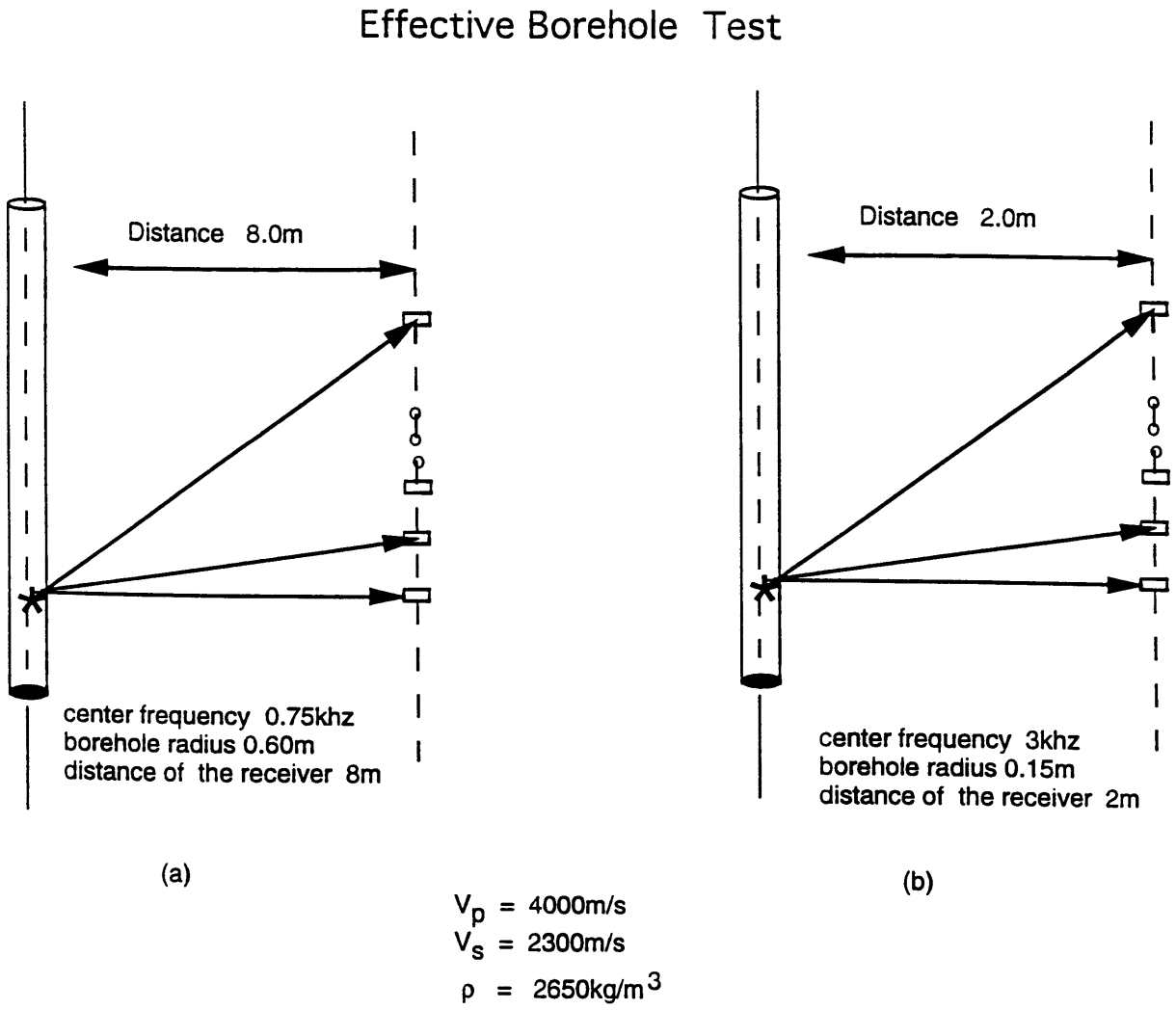

Figure 2.4: Two boreholes in the fast formation. Distances are scaled so that they remain constant in terms of wavelengths. 23 receivers are evenly distributed with spacing 1.0 m for (a) and 0.25 m for (b). Source is monopole.

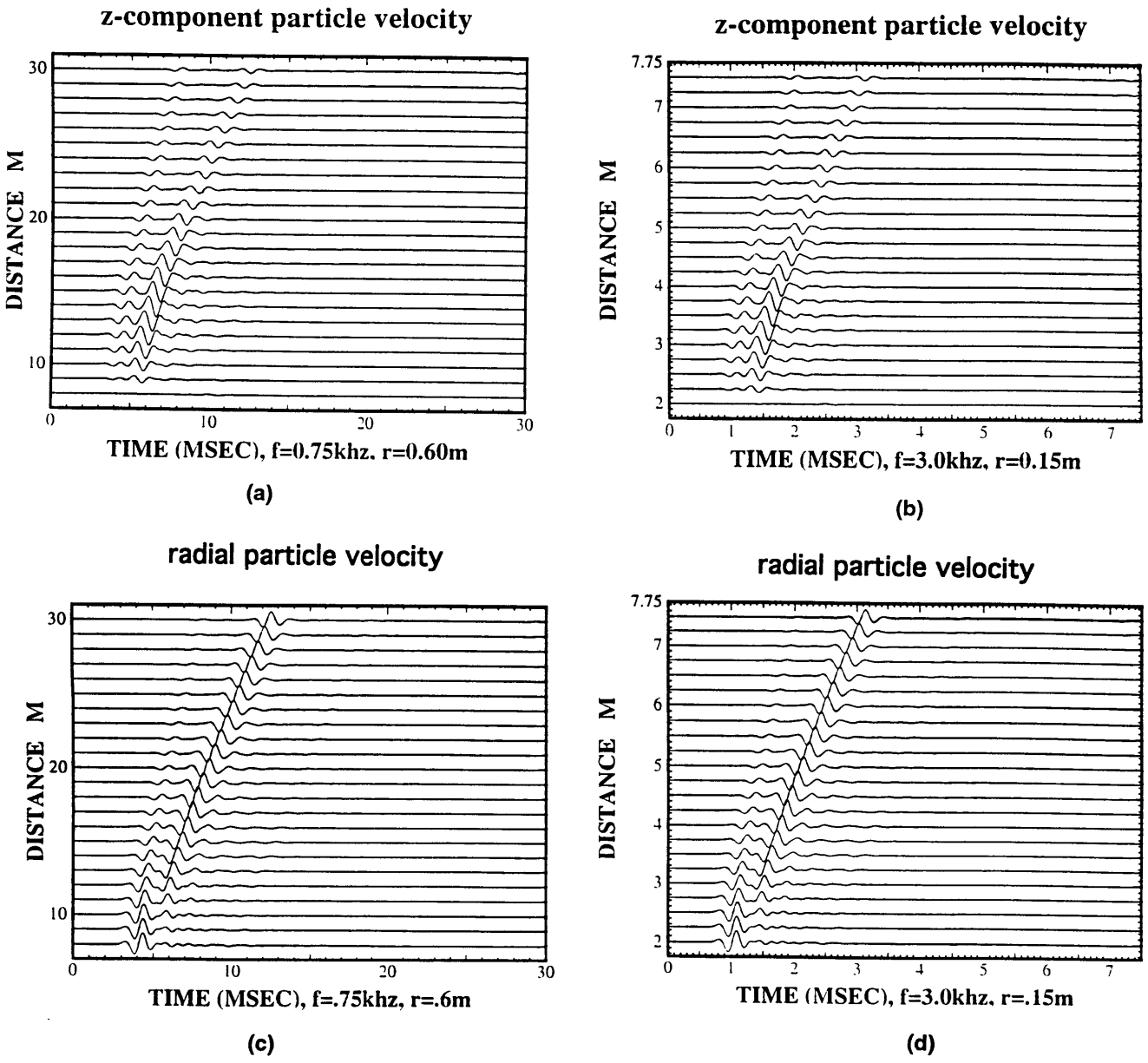

Figure 2.5: The radiation patterns computed by the finite difference method. The borehole geometry is shown in Figure 2.4. (a) and (b) are vertical and radial particle velocities for the model in Figure 2.4a, with frequency 0.75 kHz. (c) and (d) are the same quantities for model in Figure 2.4b, with frequency 3 kHz. The seismograms are essentially identical showing the dependence of borehole wave propagation in wavelength.

Chapter 3

Attenuating Tube Waves

3.1 Introduction

The energy radiated by a source in a fluid-filled borehole is mostly trapped in the borehole and transferred to the borehole waves, the head waves and the guided waves. Less than 1% of the total energy escapes the borehole and radiates into the formation (Ellefsen, 1990). A portion of the escaping waves may encounter a dipping formation in the subsurface, such as a fault or salt dome, and then reflect. The reflections then may return to the borehole. These reflected waves carry information from relatively distant subsurface structures and can be utilized to image the formation subsurface structures around a single borehole.

The utilization of the reflected waves for single-well imaging requires the separation of these from the borehole direct arrivals. However, this is difficult without attenuating the tube waves, because the energy of the tube waves is much stronger than the reflected waves (Figure 3.1). Basically, the Stoneley wave and the pseudo-Rayleigh wave (Toksöz *et al.*, 1984) are the two dominant guided waves in a fluid-filled borehole in a fast formation. The pseudo-Rayleigh waves attenuate rapidly in low frequency range due to a cut-off frequency generally around 7 to 8 kHz. In a slow formation there is no pseudo-Rayleigh wave. Although the Stoneley wave at-

tenuates exponentially away from the fluid-solid borehole wall (both in the formation and the solid formation), it does not attenuate very much while propagating along the borehole. If the Stoneley wave arrives after the reflected waves, Chen *et al.* (1994) suggested separating the reflections by choosing an appropriate time window. In most cases the borehole waves arrive before the reflected arrivals, and the reflected waves are strongly contaminated by the Stoneley waves. It is therefore difficult to identify the reflected waves and separate them from the dominant tube waves. The difficulty imposes the importance of investigating a way to artificially block the Stoneley wave in real borehole imaging.

It has been reported that the petroleum industry has tried to use tube wave dampers to attenuate the borehole Stoneley wave. But, to our knowledge there is no theoretical or quantitative analysis to investigate how the dampers work and how the physical and geometrical properties of the dampers affect the attenuation of the tube waves, and how to design the best tube wave damper according to formation properties, the source center frequency, and the borehole geometry. In this chapter we investigate these effects with the finite difference method.

3.2 Numerical Simulation

The damper model and the borehole geometry are shown in Figure 3.2a. In our numerical modeling, the tube wave damper is simply modeled as a hollow cylinder. The monopole source is located in the center of the borehole of radius 15 cm. Receivers are evenly located upward along the borehole axis, and go through the damper to detect the tube waves and the changes when a tube wave damper is applied. The objective of the modeling is to investigate the effects of the damper material and geometry on the attenuation of the Stoneley wave.

3.2.1 Effect of Damper Rigidity

Four types of material are used as dampers and their physical properties are shown in Table 3.1. All dampers have the same damper geometry—a hollow cylinder with inner radius of 3 cm and outer radius of 15 cm and length of 10 cm.

Damper Material Properties

	$V_p\ m/s$	$V_s\ m/s$	$\rho\ kg/m^3$
highest rigidity	5970	3300	3300
high rigidity	5000	3000	3000
medium rigidity	2000	1000	1200
fluid	1000	0	500

Table 3.1: Physical properties of materials used in the tube wave damping numerical tests. Physical properties include P-wave (V_p) and S-wave (V_s) velocities, densities (ρ), The Velocities are in meters per second, densities in kilograms per cubic meters.

Synthetic seismograms for the high rigidity damper show clearly the attenuation of the tube waves (Figure 3.2b). Amplitudes of the tube waves picked from these seismograms and the analogous results for other materials show the effect of the material rigidity on the attenuation of the tube waves (Figure 3.3). The curves are the maximum amplitudes of each trace vs. the receiver number. The first receiver is the nearest and the last receiver is the farthest. As we can see, if no damper is applied there is no attenuation of the Stoneley wave. This is expected since the Stoneley wave attenuation depends primarily on borehole fluid attenuation, and in our modeling we assume fluid to be water with no attenuation. In the presence of a tube wave damper, the Stoneley wave is reflected back toward the source and generally has the maximum amplitude between the source and the damper. The harder the material, the better the damper's attenuating effect. The best damper is the one made of the highest rigidity material. But there is no significant difference between the highest rigidity

damper and the high rigidity damper. This is easy to explain. It is the reflection at the damper-fluid interface that attenuates the Stoneley wave. So the attenuating effect is dependent on the reflectivity of the damper-fluid interface, which is determined by the acoustic impedance contrast of the damper and the borehole fluid. Since the difference between the acoustic impedances is small, the corresponding difference of the attenuating effect on the tube waves is also small.

If the borehole damper is a fluid with density even less than that of the borehole fluid, the Stoneley wave energy increases after the application of the damper. Although such a damper is not that realistic, the phenomenon is interesting. There are only weak reflections from the two fluid boundary and so most of the Stoneley energy is transmitted through the fluid damper. Second, part of the body wave energy propagating as refracted waves around the borehole is transferred to the Stoneley wave inside the damper. A decrease of Stoneley amplitude above the damper is due to interference of a small reflected wave. Since the velocity contrast is negative, the reflection is of opposite polarity for the incident wave, and superposition then generates a reduction in amplitude. We will use the high rigidity damper in the following numerical experiments to evaluate how the length and other properties influence the tube wave attenuation.

3.2.2 Tube Wave Damper Length

Four tests are conducted to investigate the effects of the damper length on the attenuation of the tube waves. The borehole geometry is shown as in Figure 3.2. The source center frequency is 2.0 kHz. All the dampers are made of high rigidity material (V_p = 4000 m/s, V_s = 2300, ρ = 2657 kg/m^3). The damper lengths are 5, 10, and 15 cm respectively. As shown in Figures 3.4a and 3.4b, the longer the damper, the better the tube wave attenuation. But the attenuation effects for dampers 10 and 15 cm long are not large.

3.2.3 Dependence on Center Frequency of Tube Waves

In Figure 3.5 we show the effect of tube wave frequency on wave damping. As we shall see, the effects are not too strong. Both frequencies are below the cut-off frequency of pseudo-Rayleigh waves and as a result, not much energy is scattered into the pseudo-Rayleigh.

3.2.4 Multiple Dampers

Figure 3.6a shows the geometry where two dampers, separated by 70 cm, are used to attenuate tube waves. Figure 3.6b shows seismograms for two dampers. We can see after after the attenuation of the Stoneley wave by the first damper that there is further attenuation by the second. This means that for long receiver-source distances, we can attenuate the Stoneley waves an order of magnitude by setting a series of the dampers between the source and the receivers.

3.3 Summary

We have numerically investigated the effects of a tube wave dampers on the attenuation of the tube waves. The higher the damper's rigidity, the better the attenuation. Likewise, a longer damper is better. But there are cut-off values for the rigidity and the length. Large increases of the rigidity or length do not make a big difference on the attenuation. By applying a series of dampers, the Stoneley wave can be suppressed further.

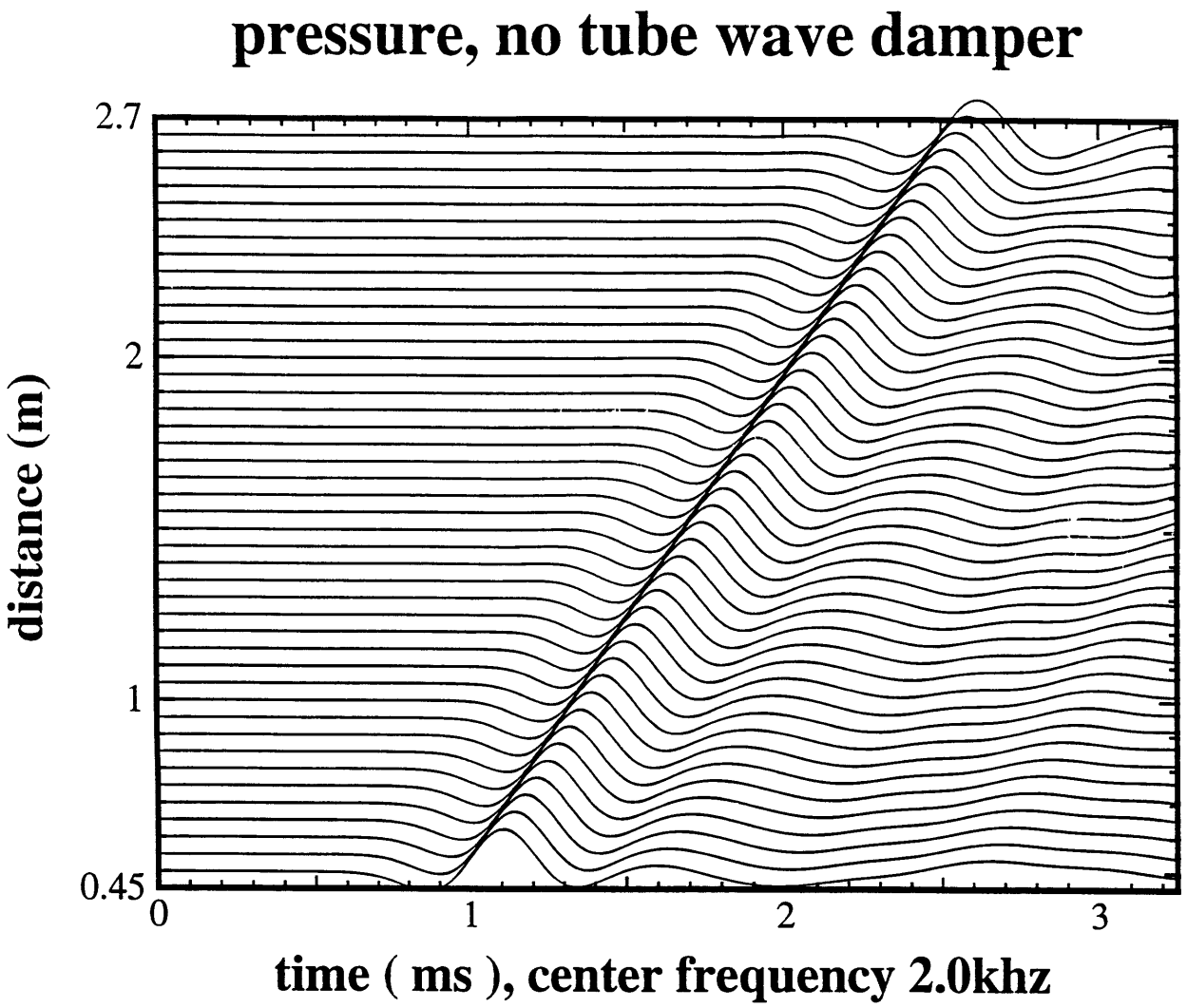

Figure 3.1 Wave propagation in a borehole of radius 15 cm, surrounded by a fast formation (Berea Sandstone, Table 2.1, Chapter 2). The center frequency is 2.0 kHz. We see essentially only the Stoneley wave, showing how strong this wave is. It will easily mask reflections in single-well experiments.

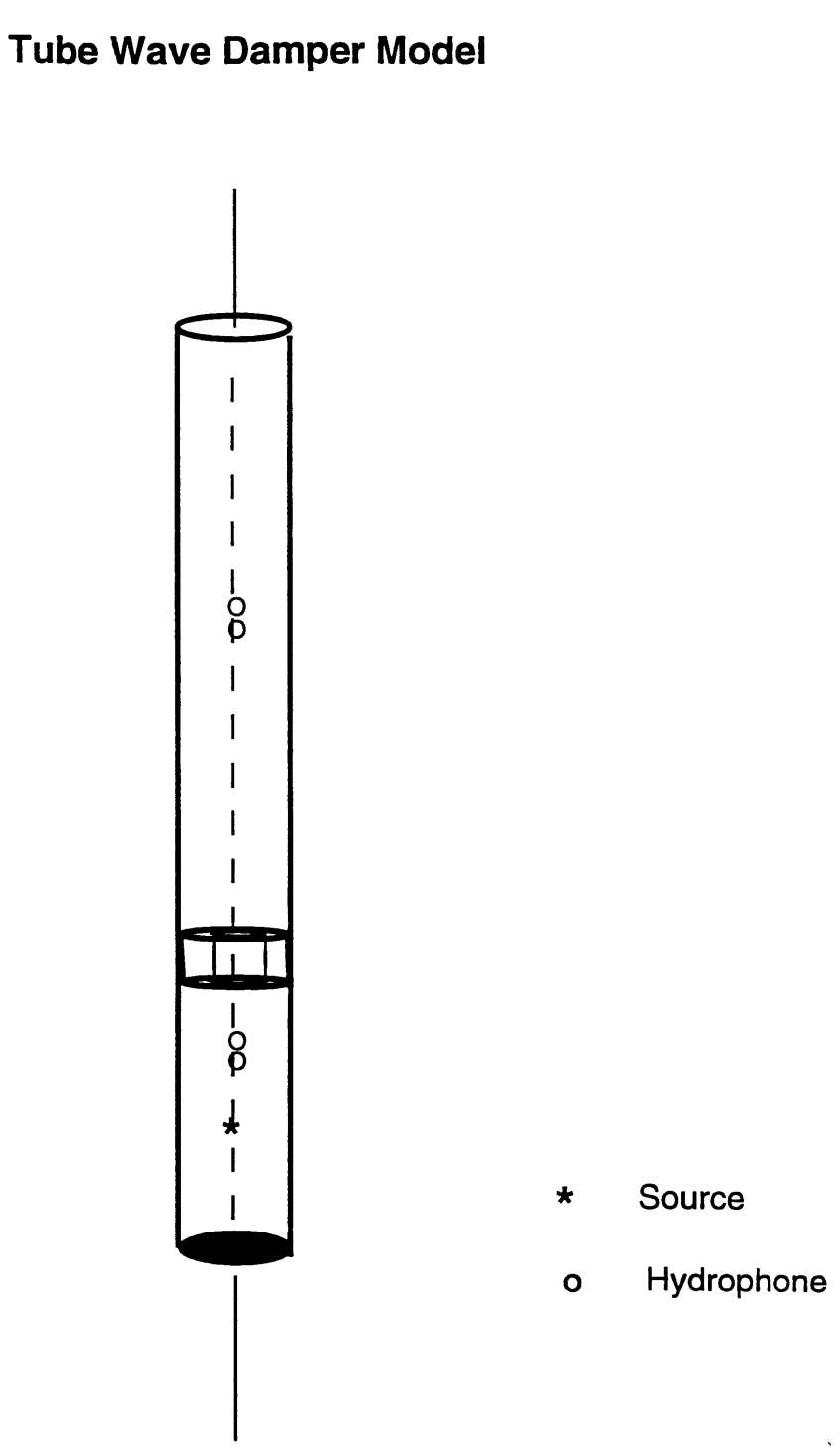

Figure 3.2a: The borehole geometry with the tube wave damper. The monopole source, with center frequency 2.0 kHz, is located in the center of the fluid-filled borehole of radius 15 cm. The cylindrical damper model is 12 cm wide (with inner radius 3 cm) hung on the borehole, with distance 35 cm from the source. Hydrophones are evenly distributed along the borehole axis with even spacing of 5 cm. The minimum source-receiver distance is 15 cm.

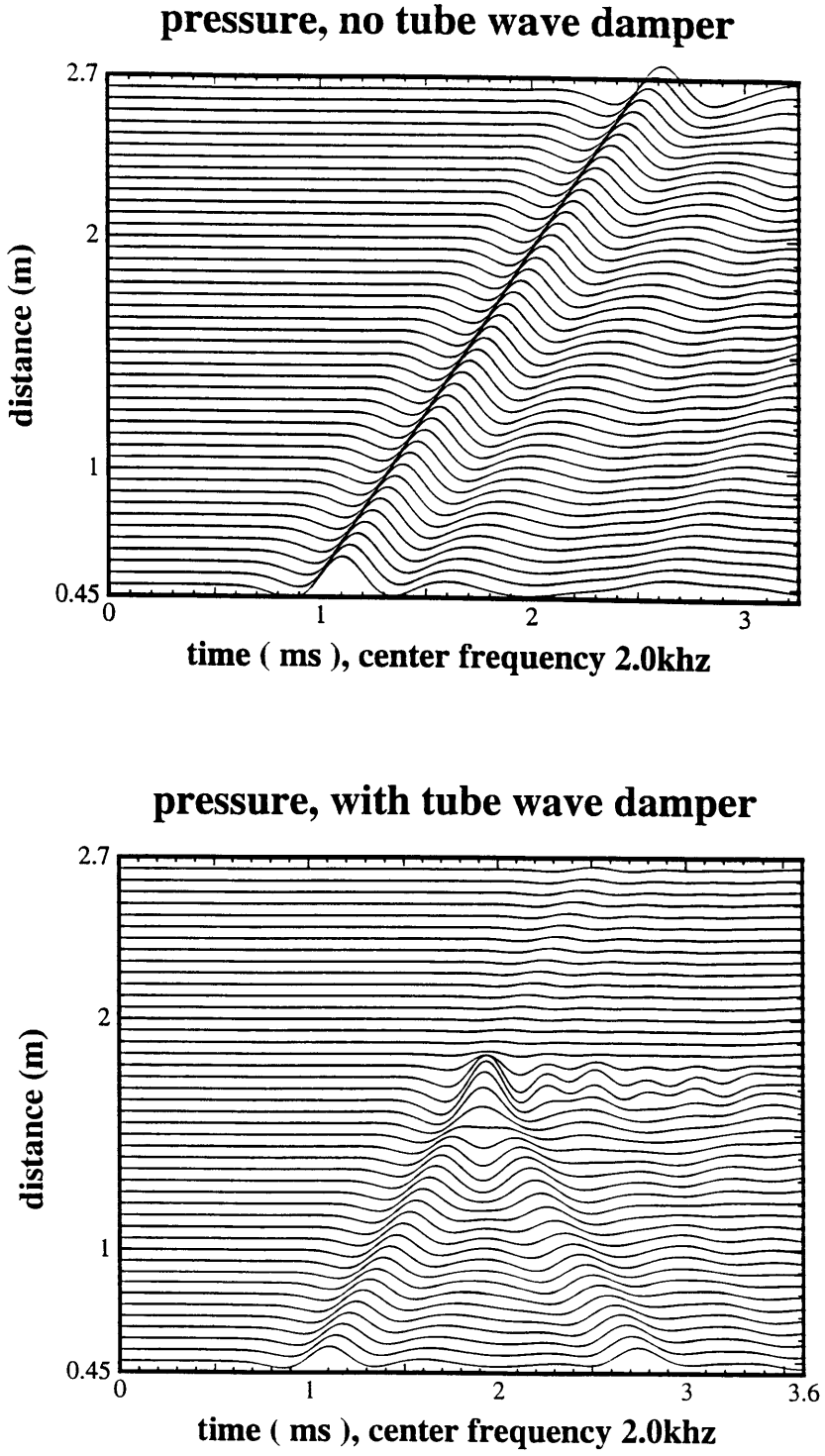

Figure 3.2b: A high rigidity damper (V_p = 4000 m/s, V_s = 2300 m/s, ρ = 2657 kg/m^3) 10 cm long and 12 cm wide, is used to attenuate the tube wave. Twenty-two receivers are evenly distributed along the borehole axis from 0.5 m to 2.65 m from the source with even spacing 0.1 m. Top: tube waves without the damper. Bottom: with the damper showing in detail the blocking of the Stoneley waves.

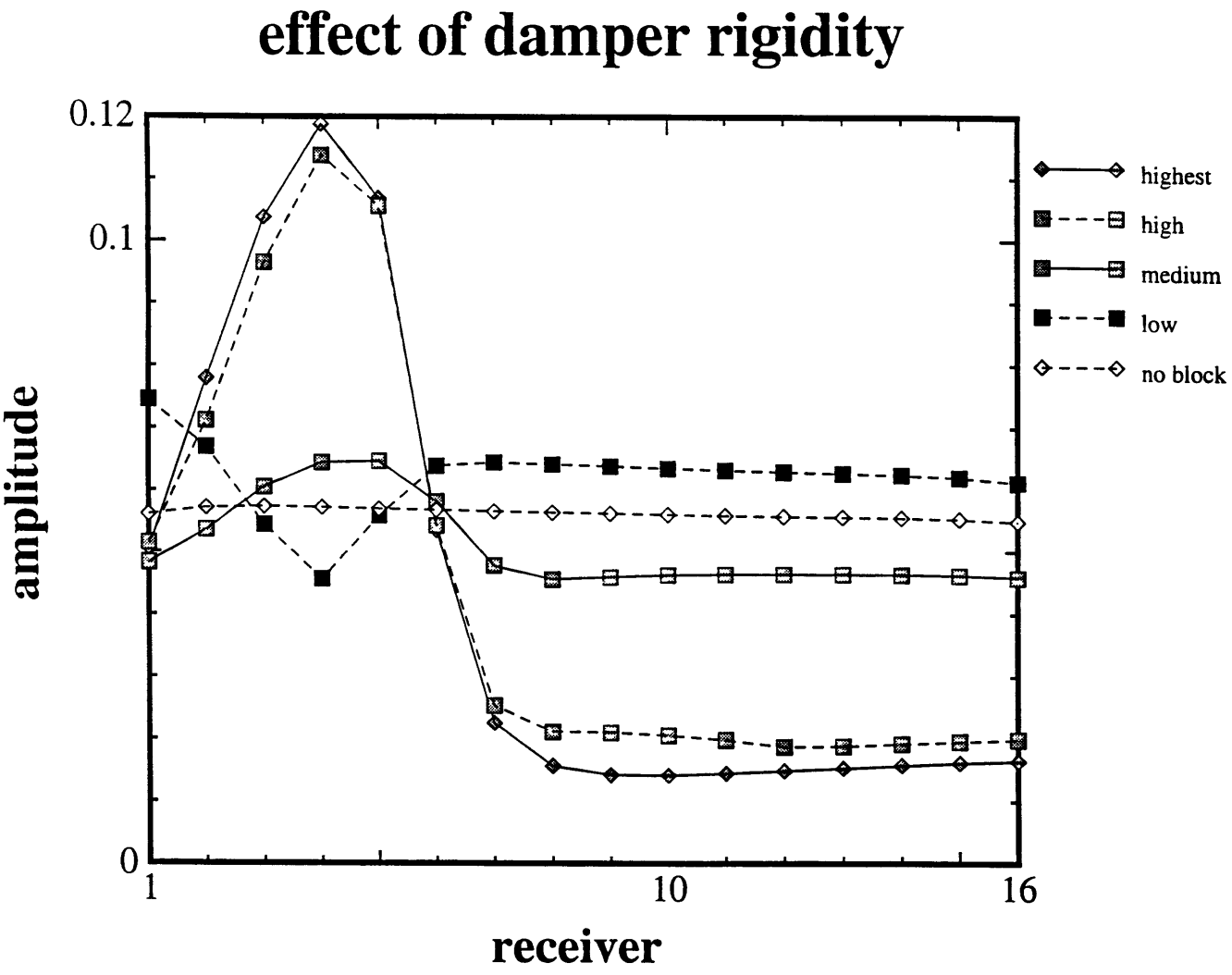

Figure 3.3a: Five numerical tests conducted to investigate the effects of damper material on the attenuation of tube waves. The damper model is a hollow cylinder touching the borehole wall. Each damper is 10 cm long, 12 cm wide (the inner radius is 3 cm and the outer radius 15 cm), with material with properties: (a) highest rigidity: $V_p = 5000$ m/s, $V_s = 3300$ m/s, and $\rho = 3000$ kg/m^3; (b) high rigidity: $V_p = 4000$ m/s, $V_s = 4000$ m/s, and $\rho = 2657$ kg/m^3; (c) medium rigidity: $V_p = 2000$ m/s, $V_s = 1000$ m/s, and $\rho = 1200$ kg/m^3; (d) a fluid: $V_p = 1000$ m/s, $V_s = 0.0$ m/s, and $\rho = 500$ kg/m^3. The borehole geometry is shown in Figure 3.1. The curves are the maximum amplitudes of each trace vs. the receiver number. The first receiver is the nearest and the last is the farthest one. The corresponding seismograms are shown in Figure 3.3b.

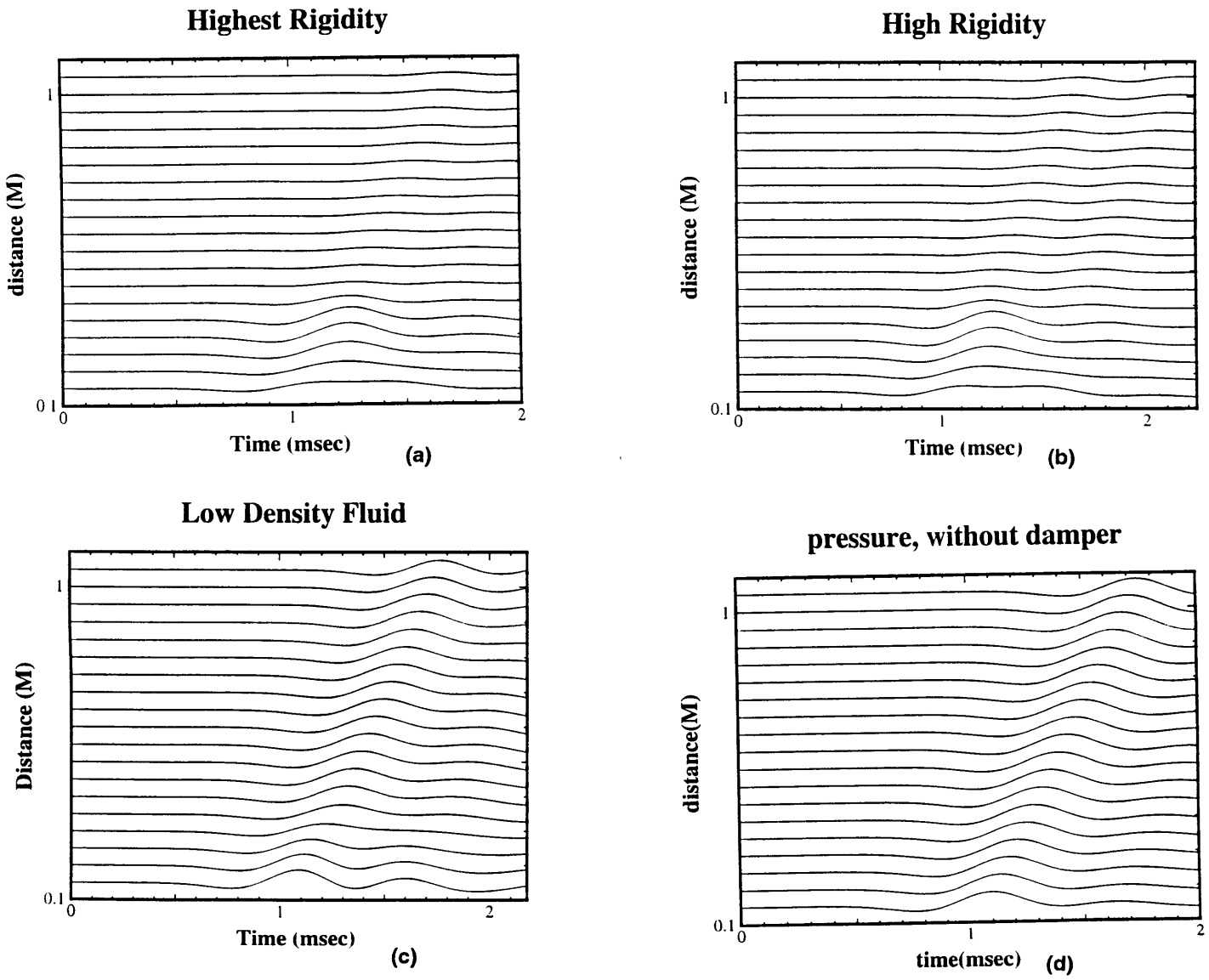

Figure 3.3b: Tube wave seismograms in borehole showing effect of the attenuation of tube waves. The material properties of the dampers are shown in the caption of 3.3a and the borehole geometry in Figure 3.2.

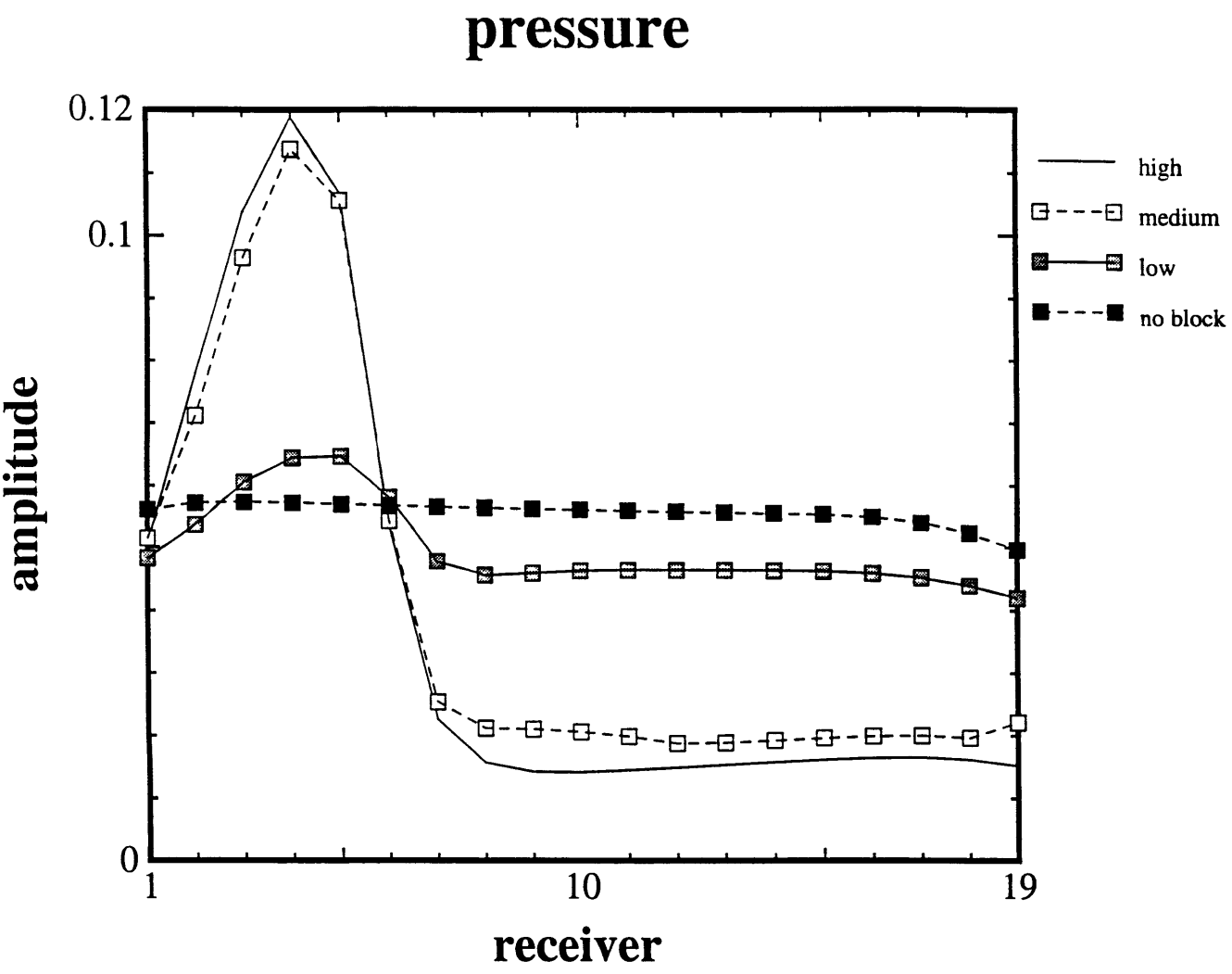

Figure 3.4a: The effects of the damper's length on the tube waves attenuating. One test without damper and the other three with dampers 5 cm, 10 cm, and 15 cm long separately. All dampers are made of high rigidity material ($V_p = 4000$ m/s, $V_s = 2300$ m/s, $\rho = 2657$ kg/m^3). The borehole geometry is shown in Figure 3.1. The curves are the maximum amplitude of each trace vs. the receiver of number. The corresponding seismograms are shown in Figure 3.4b.

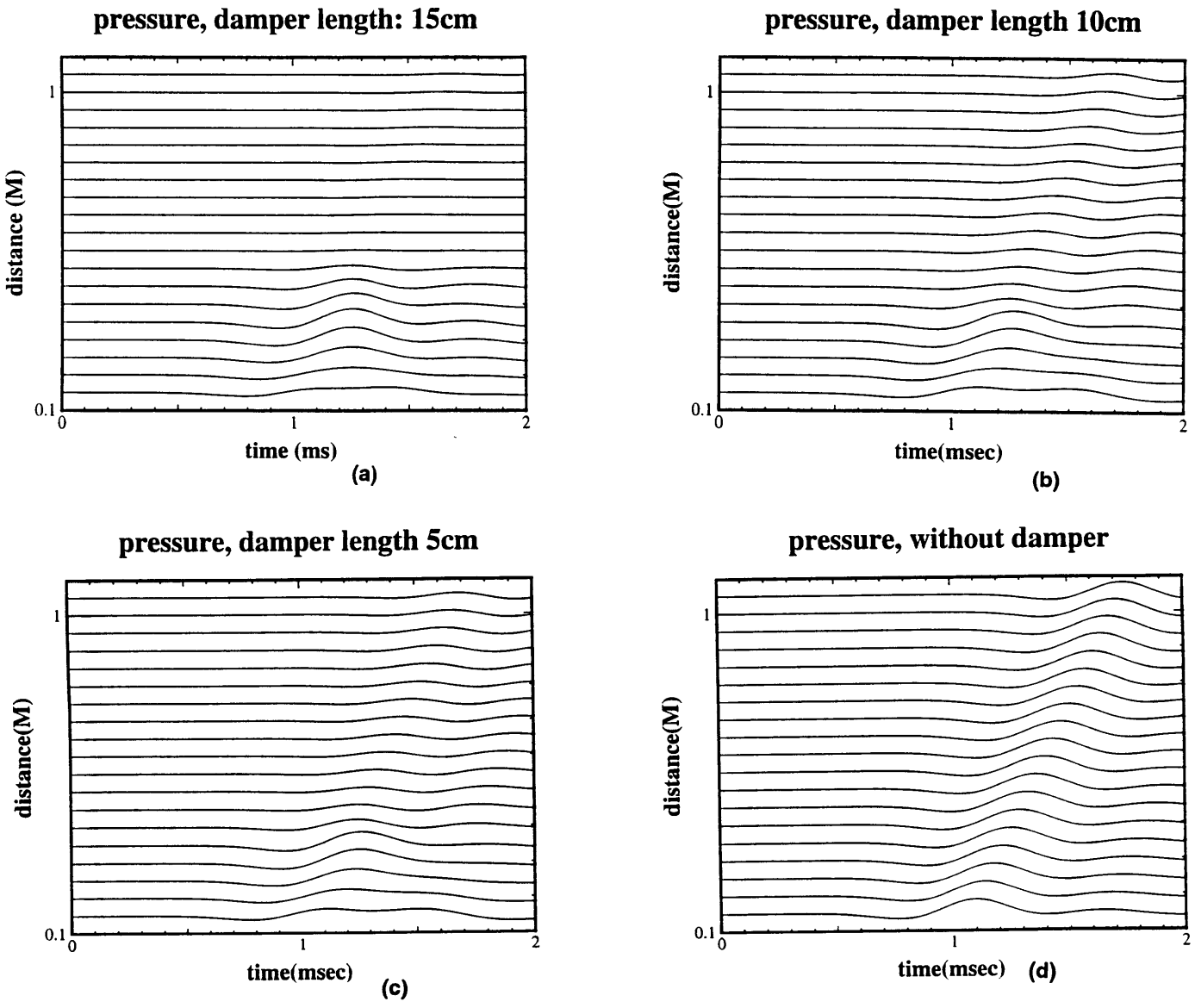

Figure 3.4b: The effects of damper length. The damper properties are shown in Figure 3.4a.

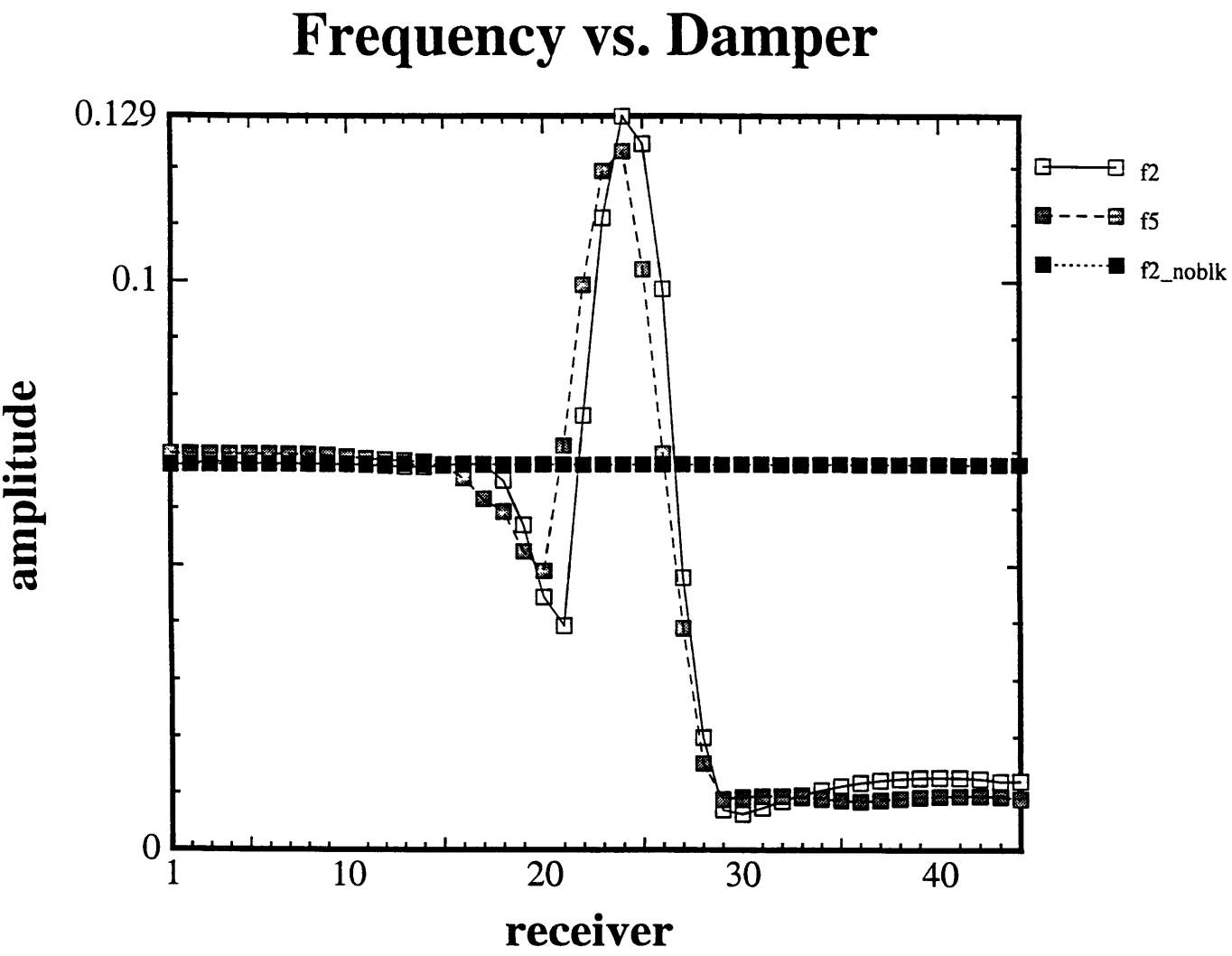

Figure 3.5: A high rigidity damper ($V_p = 4000$ m/s, $V_s = 2300$ m/s, $\rho = 2657$ kg/m^3), 10 cm long and 12 cm wide, is used for testing the relationship between the frequency and the attenuating effect of dampers on the tube wave. Frequencies of 2 kHz (f2) and 5 kHz (f5) are used, the results are compared with reference case without damper (center frequency 2 kHz, f2_noblk). The corresponding seismograms are shown in Figure 3.5b.

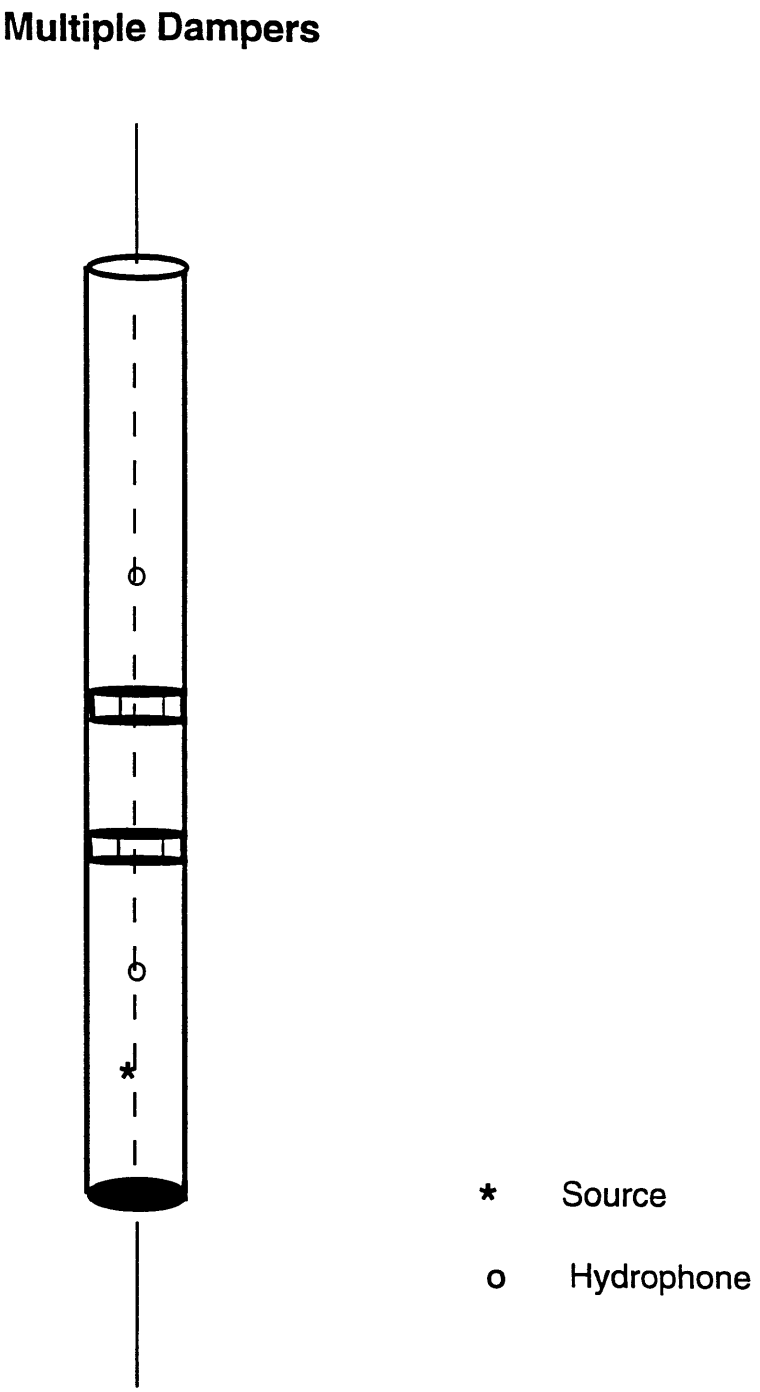

Figure 3.6a: The monopole source is located in the center of the fluid-filled borehole of radius 15 cm. Each damper is 10 cm long and 12 cm wide (inner radius 3 cm). The lower damper and the upper damper are 1.15 m and 1.85 m away from the source, respectively. 44 hydrophones are evenly distributed along the borehole axis with spacing 5 cm. The nearest source-receiver offset is 0.5 m.

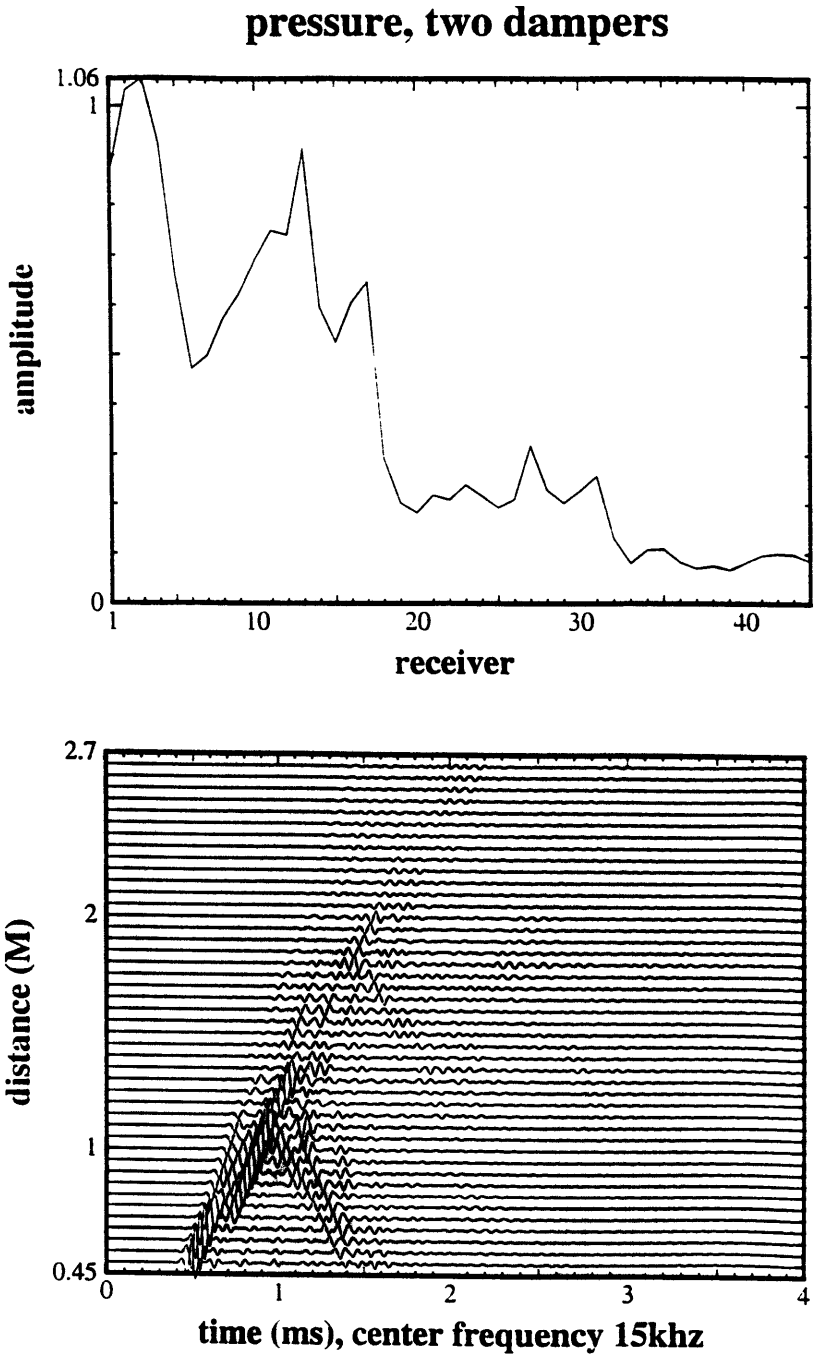

Figure 3.6b: Two high rigidity dampers ($V_p = 4000$ m/s, $V_s = 2300$ m/s, $\rho = 2657$ kg/m^3), each 10 cm long and 12 cm wide, are used. The center frequency is 15 kHz. Top: maximum amplitudes of each trace. Bottom: pressure seismogram.

Chapter 4

Conclusions

Single-well imaging requires the utilization of sources in a borehole and recording of reflected waves in the same borehole to infer subsurface structures. A major difficulty in modeling wave propagation in this situation is that a direct, conventional incorporation of the source/receiver borehole in 3-D finite difference codes requires a very fine model discretization. The borehole is small, though propagation distances can be large, and so computation cost then becomes prohibitive. We proved that these constraints can be relaxed somewhat under realistic conditions in two ways: (1) at lower frequencies (hundreds of Hertz), the borehole can be modeled using as few as 4 points per radius; and (2) the model size of the borehole can be increased without significantly changing the radiation patterns as long as wavelength relative to borehole size is still fairly large.

There are additional difficulties in single-well imaging, in that it is difficult to implement because the reflected waves are generally contaminated by large amplitude tube waves. To overcome this difficulty it is important to artificially block the tube waves. In the second part of this thesis, we use the three-dimensional finite difference calculation to simulate the tube wave dampers in the borehole. A damper is simply modeled as a hollow cylinder touching the borehole wall. We investigated the effects of the damper's geometrical properties and material rigidity on the attenuating of the

Stoneley waves.

The primary effect of mechanical dampers is to block transmission of the tube wave by scattering the incident tube waves. At long wavelengths corresponding to frequencies of 2 kHz or below, the damper act as as a reflector. Hence, the tube wave attenuation depends on the damper's acoustic impedance, the cross-sectional area, and length. The higher the rigidity of the damper material, the better the attenuation. Reflection coefficients are roughly proportional to the cross-section area of the damper. For optimum attenuation the damper length should be at least 10 cm. A further increase of the length does not make a big difference in the attenuation. The use of multiple dampers between the source and the receivers attenuates tube waves more than a single. This may hold the promise to suppress the tube waves sufficiently before the seismic processing to extract the reflected waves.

Further research direction is necessary to evaluate the other aspects of single hole imaging. In this thesis, the main effort was to focus on effectively using the finite difference method to model the mechanical borehole dampers to block the borehole tube waves. For simplicity, the study was limited to the low frequency monopole source and homogeneous formation and simple structures. Further research needs to include cased holes, complex structures, and more extensive modeling to generate suites of seismograms and processing of data to separate the reflected waves for imaging of the geologic features.

REFERENCES

Abdalla, A.A., Stewart R.R., and Henley, D.C.,1990, Traveltime Inversion and reflection processing of crosshole seismic data, *60th Ann. Internat. Mtg., Soc. Expl. Geophys., Expanded Abstracts*, 47–50.

Baker, L.J. and Harris, J.M., 1984, Cross-borehole seismic imaging, presented at the 54th Ann. Internat. Mtg., Soc. Expl. Geophys.

Beydoun, W.B. and Delvaux, J.M., 1989, Elastic ray-Born 12-migration/inversion, *Geophys. J., 97*, 151–160.

Beydoun, W.B., Delvaux, J., Mendes, M., Noual, G., and Tarantola, A., 1989, Practical aspects of an elastic migration/inversion of crosshole data for reservoir characterization: A Parais basin example, *Geophysics, 54*, 1587–1595.

Chen, S.-T., Miller, M.A., and Zimmerman, L.J., 1994, Single-well profiling tool with a variable downhole source/receiver spacer, *64th Ann. Mtg., Soc. Expl. Geophys., Expanded Abstracts*, 303–306.

Cheng, N.Y., 1994, Borehole wave propagation in isotropic and anisotropic media: Three-dimensional finite difference approach, Ph.D. thesis, Massachusetts Institute of Technology, Cambridge, MA.

Clayton, R. and Engquist, B., 1977, Absorbing boundary conditions for acoustic and elastic wave equations, *Bull. Seis. Soc. Am., 67*, 1529–1540.

Devaney, A.J., 1984, Geophysical diffractional tomography, *IEEE Trans. Geosci. Remote*

Sensing, GE-22, 3–13.

Dickens, T.A., 1994, Diffraction tomography for crosswell imaging of nearly layered media, *Geophysics, 59*, 694–706.

Dong, W., 1993, Elastic wave radiation from borehole seismic sources in anisotropic media, Ph.D. thesis, Massachusetts Institute of Technology, Cambridge, MA.

Dong, W., M. Bouchon, and M.N. Toksöz, 1992, Modeling downhole source radiation by boundary element and discrete wave number method, in *63th Ann. Internat. Mtg., Soc. Expl. Geophys., Expanded Abstracts*, 1339–1340.

Ellefsen, K.J., 1990, Elastic wave propagation along a borehole in an anisotropic medium, Ph.D. thesis, Massachusetts Institute of Technology, Cambridge, MA.

Gibson, R.L., 1994, Radiation from seismic sources in cased and cemented boreholes, *Geophysics, 59.*

Heelan, P., 1953, Radiation from a cylindrical source of finite length, *Geophysics, 18*, 685–695.

Hidgon, R.L., 1986, Absorbing boundary conditions for difference approximations to the multi-dimensional wave equation, *Mathematics of Computation, 47*, 437–459.

Hidgon, R.L., 1987, Numerical absorbing boundary conditions for the wave equation, *Mathematics of Computation, 49*, 65–90.

Hidgon, R.L., 1990, Radiation boundary conditions for elastic wave propagation, *SIAM J. Numer. Anal., 27*, 831–870.

Hornby, B.E., 1989, Imaging of near-borehole structure using full-waveform sonic data, *Geophysics, 54*, 747–757.

Hornby, B.E., 1993, Tomographic reconstruction of near-borehole slowness using refracted borehole sonic arrivals, *Geophysics, 58*, 1726–1736.

Hu, L., McMechan, G.A., and Harris, J.M., 1988, Acoustic prestack migration of cross-hole data, *Geophysics, 53*, 1015–1023.

Iverson, W.P., 1988, Cross-well logging for acoustic impedance, *Petrol. Tech. J., 40*, 75–82.

Kelly, K.R., Ward, R.W., Treitel, S., and Alford, R.M., 1976, Synthetic seismograms: A finite-difference approach, *Geophysics, 41*, 115–135.

Kurkjian, A.L., Coates, R.T., White, J.E., and Schmidt, H., 1994, Finite-difference and frequency-wavenumber modeling of seismic monopole sources and receivers in fluid-dilled boreholes, *Geophysics, 59*, 1053–1064.

Lee, M. and Balch, A., 1982, Theoretical seismic wave radiation from a fluid-filled borehole, *Geophysics, 49*, 27–36.

Levander, A.R., 1988, Fourth-order finite difference P-SV seismograms, *Geophysics, 53*, 1425–1436.

Lindman, E.L., 1975, Free-space boundary conditions for the time dependent wave equation, *J. Comput. Phys., 18*, 66–78.

Lo, T.W., Toksöz, M.N., Xu, S., and Wu, R.S., 1988, Ultrsonic laboratory tests of geophysical tomographic reconstruction, *Geophysics, 53*, 947–956.

Meredith, J., Cheng C.H., Toksöz, M.N., and Bouchon, M., 1990, Near field radiation from a downhole point seismic source, in *SEG Annual Meeting Expanded Technical Program Abstracts.*

Peng, C., 1993, Borehole effects on downhole seismic measurements, Ph.D. thesis, Massachusetts Institute of Technology, Cambridge, MA.

Pratt, R.G. and Worthington, M.H., 1990a, Inverse theory applied to multisource crosshole tomography, Part 1. Acoustic wave-equation method, *Geophys. Prosp., 38*, 287–310.

Pratt, R.G. and Worthington, M.H., 1990b, Inverse theory applied to multisource crosshole tomography, Part 2: Elastic wave equation method, *Geophys. Prosp. 38*, 311–329.

Thomsen, L., 1986, Weak elastic anisotropy, *Geophysics, 51,* 1954–1966.

Toksöz, M.N., Cheng, C.H., and Willis, M.E., 1984, Seismic waves in a borehole—a review, in *Vertical Seismic Profiling: Advanced Concepts, vol. 14B*, M.N. Toksöz and R. Stewart (eds.), in *Handbook of Geophysical Explanation*, K. Helbig and S. Treitel (eds.), Geophysical Press, London, 256–275.

Virieux, J., 1984, SH-wave propagation in heterogeneous media: Velocity-stress finite-difference method, *Geophysics, 49,* 1933–1957.

Virieux, J., 1986, P-SV wave propagation in heterogeneous media: velocity-stress finite-difference method, *Geophysics, 51*, 889–891.

Wu, R.S., and Toksöz, M.N., 1987, Diffraction tomography and multisource holography applied to seismic imaging, *Geophysics, 52*, 11–25.